04

Experimental stand for studying the characteristics of powerful laser-plasma sources of EUV radiation

© A.A. Perekalov, V.E. Guseva, A.N. Nechay, N.I. Chkhalo, P.A. Veprev, A.I. Artyukhov

Institute of Physics of Microstructures, Russian Academy of Sciences,
607680 Nizhny Novgorod, Russia
e-mail: perekalov@ipmras.ru

Received May 29, 2025
Revised May 29, 2025
Accepted May 29, 2025

The design and characteristics of a setup for studying powerful laser-plasma sources of extreme ultraviolet radiation are described. A pulsed Nd : YAG- laser with a pulse duration of 5.2 ns, pulse energy of up to 0.7 J and a pulse repetition rate of 10 Hz is used to form a laser spark. A supersonic gas jet of Xe formed by a conical nozzle equipped with a pulse valve. The diameter of the critical section of the nozzle is 500 μm, the length is 5 mm, the half-angle of the cone aperture is 4.5°. To study high-power laser-plasma sources, it is planned to equip the setup with conical nozzles with a critical section diameter of 200−300 μm without a pulse valve and a laser system with a pulse repetition rate of 1 kHz and higher. A high-performance pumping system with a total capacity of 9000 l/s allows maintaining a high vacuum level and conducting research in conditions close to the operating conditions of radiation sources for the new generation of lithographs being designed.

Keywords: laser plasma, EUV radiation, gas-jet targets, conversion efficiency.

DOI: 10.61011/TP.2025.09.61835.70-25

Introduction

Due to significant progress in a technology of sputtering of multilayer X-ray mirrors (MXM) and synthesis of Be--containing mirrors with high (at the level of 72 %) reflectances at the wavelengths around 11.2 nm [1–3], an idea was put forward about the possibility of creating a new-generation extreme ultraviolet (EUV) lithograph. It is expected to use a laser-plasma source (LPS) of EUV radiation with a gas-jet Xe target in this lithograph. When using inert Xe as the target, it is possible to design a „clean" radiation source, thereby making it possible to solve one of the key problems of the sources with tin-based targets, i.e. contamination of optical elements with target destruction products, and at the same time to obtain high radiation power in the EUV range. At the same time, as shown in the study [4], performance of the lithograph with the LPS based on the Xe-target at the wavelength of 11.2 nm can be at the level of performance achieved on the lithograph with the wavelength of 13.5 nm, which uses the tin target.

By now, the LPSes with the gas-jet Xe target have been investigated in a quite large number of the studies [5–7]. Besides, conversion efficiency (CE) of this source has been measured at the wavelengths 11.2 and 13.5 nm [8–11]. The most studies were carried out using cheap laboratory laser systems that are characterized by quite high pulse energy of about 1 J and a pulse repetition rate of about 10 Hz. The radiation sources based on such lasers with low time-average radiation power are designed and applied in installations for mask diagnostics, metrology, etc. [12,13].

In order to create the high-performance EUV lithograph, it is required to have a radiation source with high average power. For the LPSes, the most optimal method of increasing the source power is to use laser system with the high pulse repetition rate above 1 kHz. In this operation mode, the gas-jet target can be formed in a vacuum volume only by means of nozzles with continuous gas outflow (without a pulse valve). At this, gas flowrates will be quite high, therefore, in order to achieve a low residual pressure level in the vacuum chamber (at most 10^{-3} Torr), it is necessary to equip the source with a powerful pump-out system. In the worst vacuum conditions, effective power of the LPS will be reduced due to absorption of EUV radiation by residual xenon in the vacuum chamber [5].

The present study describes a design, operating principles and characteristics of a test stand for studying the characteristics of power laser-plasma sources of EUV radiation. This stand is equipped with the powerful pump-out system, thereby making it possible to carry out the studies in experimental conditions that are close to the operating conditions of the radiation source in a designed new-generation lithographic machine. The present study describes the first results of measurements of conversion efficiency of the LPS with the gas-jet Xe target, which are obtained in this stand.

1. Design and characteristics of the stand

A principal diagram of the test stand is shown in Fig. 1 and a photo of the stand is shown in Fig. 2. The gas-jet target is formed by supersonic outflow of the gas jet into a volume of the vacuum chamber through a conical nozzle. A

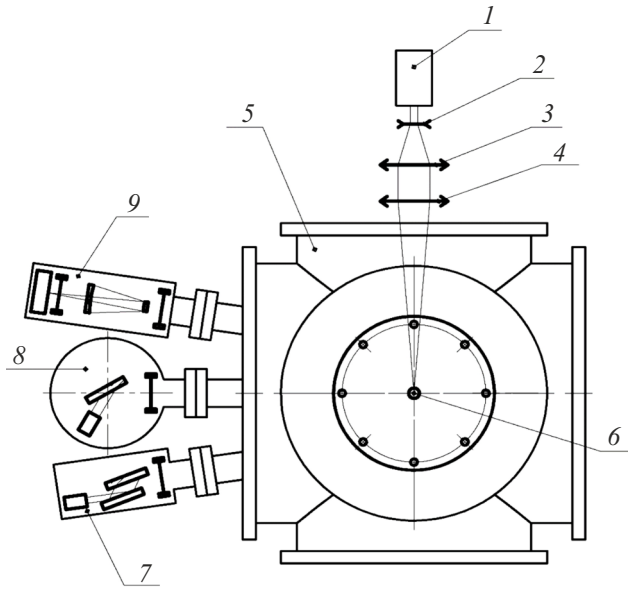

Figure 1. Diagram of the experimental stand: *1* — theNd : YAG-laser, *2* — the diverging lens, *3* — the converging lens, *4* — the long-focus lens, *5* — the vacuum chamber, *6* — the laser spark, *7* — the double-mirror monochromator, *8* — the mirror spectrometer, *9* — the EUV imaging system.

Figure 2. Photo of the experimental stand.

plasma cloud is formed by using laser radiation *1*. Radiation of the laser that operates in a pulsed mode is transmitted through a three-element focusing lens, which consists of a diverging *2*, a converging *3* and a long-focus *4* lens. When the source operates, a point of focus of the optical system is arranged in the gas jet, thereby resulting in ionization of gas atoms and formation of the plasma cloud and a laser spark *6*. Presently, the EUV radiation diagnostics system consists of three main components: a double-mirror monochromator *7*, a mirror spectrometer *8*, an imaging system *9*. All the used X-ray mirrors are manufactured based on the Mo/Be-structure and optimized to operate at the wavelength of 11.2 nm.

The volume of the vacuum chamber is depressurized by three turbomolecular pumps of performance of 3000 l/s each. Due to using the high-performance pump-out system, it is possible in this stand to achieve a low residual pressure level in the chamber of at most 10^{-3} Torr during formation of the target due to the permanent-outflow conical nozzles with the critical-section diameter $d_{cr} = 200-300\,\mu$m and the length $L = 5-15$ mm without using the pulse valve. This operation mode makes it possible to study the LPS characteristics in the conditions that are close to the conditions of operation of the designed new-generation lithographic machine (using the laser systems with the pulse repetition rate of 1 kHz and more).

Presently, there is a final stage of designing an ion spectrometer designed to study spatial distribution of ion fluxes and an energy spectrum [14] and a small-size high-resolution spectrograph [15].

1.1. Laser-optical system

Presently, the main element of the laser-optical system of the stand is a Nd : YAG-laser with pulse duration of 5.2 ns and pulse energy of up to 0.7 J and the pulse repetition rate of 10 Hz. A diameter of a laser output beam is 10 mm. Operations of the laser and the nozzle's pulse valve are synchronized by means of a master oscillator.

In its optical path, the laser beam is transmitted through the three-element focusing lens (Fig. 3). The lens consists of a beam expander that includes a diverging and converging lenses made of the glass VK-7, while the beam diameter increases from 10 to 38 mm. The diverging lens is spherical and plano-concave. Its diameter is 25.4 mm, the curvature radius of the spherical surface is 79.5 mm and the focal distance is $f = -150$ mm. The converging lens is spherical and plano-convex. The lens diameter is 50.8 mm, the curvature radius of the spherical surface is 234 mm and the focal distance is $f = 450$ mm. The diverging and converging lenses are separated by a distance of 300 mm from each other so that to ensure parallelism of the beam that outgoes from the converging lens. Then the expanded parallel beam of the diameter of 38 mm is focused by the long-focus lens that is also made of the glass VK-7. This lens is plano-convex, its diameter is 50.8 mm, the curvature radius of the spherical surface is 257 mm and the focal distance is $f = 500$ mm. A surface of all the three lenses have

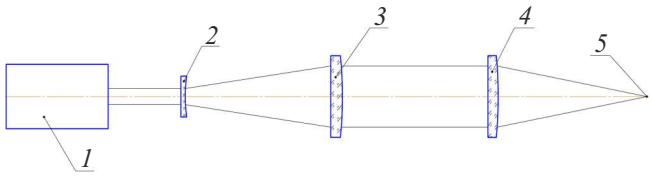

Figure 3. Diagram of the three-element focusing lens: *1* — the Nd : YAG-laser, *2* — the diverging lens, *3* — the converging lens, *4* — the focusing lens, *5* — the focus point.

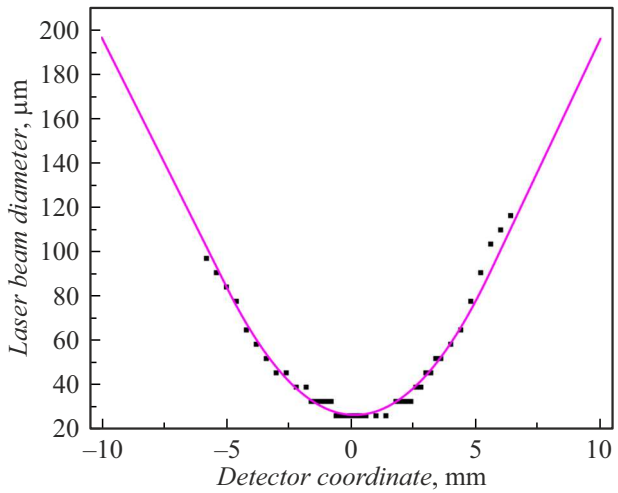

Figure 4. Results of measurement of the laser beam diameter by means of the CCD camera.

an antireflection coating for the wavelength of 1064 nm applied in order to reduce reflection of laser radiation from the surfaces of the lenses and, respectively, to reduce the energy of radiation reaching the target. The focusing lens is arranged on a linear translator designed to move it within $+-20$ mm from the nominal position. Thus, it is possible to irradiate the gas-jet target both with an acutely focused and a defocused beam.

Before the main experiments, we have measured sizes of a focusing spot of laser radiation, which is obtained by means of the three-element lens. In order to measured the spot size, a radiation detector was placed in the area near the focus. The detector was a CCD camera BMR-1400HM-U with the pixel size of 6.45 μm. The CCD camera was placed on the linear translator designed to move the camera along the focus system within $+-10$ mm from the nominal position, and a positioning accuracy is at most 0.05 mm. The laser radiation was attenuated by means of special filters upstream of a lens input and downstream of the focusing lens. The filters are required to reduce the power of incident laser radiation by several orders and to prevent destruction of a sensitive element of the detector. The measurement results were taken to obtain a dependence of the laser ray sized on the position of the CCD camera, as shown in Fig. 4.

It is clear from the dependence of Fig. 4 that the diameter of a „waist“ of the laser beam is $d = 25\,\mu$m, while a waist length is $L = 1.5$ mm. The laser ray diameter was measured by laser beam images that are averaged along 30 pulses, at the level of 0.5 of the maximum value of the signal (FWHM). Thus, when taking into account the laser pulse, the power density in the focus spot is about 10^{13} W/cm^2.

In the future, it is planned to study the LPS characteristics with the gas-jet Xe target in a dependence on laser pulse duration from tenths of ns to several tens of ns. After that, it will be possible to carry out works on LPS investigation in the test stand, wherein plasma is formed therein by using the laser system with the pulse repetition rate of at least 1 kHz. These experiments are necessary for detailed investigation of the characteristics of the LPS designed for the new-generation EUV lithograph.

1.2. Target formation system

Now, the main element of the target formation system is a conical supersonic nozzle with the critical-section diameter $d_{cr} = 500\,\mu$m, the length $L = 5$ mm and the half-angle of the cone aperture $\alpha = 4.5°$. The nozzle is additionally equipped with the pulse valve based on an injector Bosch 0 280 158 017. The maximum gas pressure, at which this system can operate, is 25 bar. The nozzle is fixed on a three-coordinate slide, thereby providing its displacement inside the vacuum chamber along the three axes of coordinates. The nozzle positioning accuracy is 0.05 mm.

In perspective, this test stand can be used to investigate the systems of formation of the gas-jet targets based on the conical nozzles that have the smaller critical-section diameter and are not equipped with the pulse valve. It is also possible to investigate the gas jets that are formed by capillaries and specially-profiled nozzles.

1.3. Vacuum pump-out system

The test stand is equipped with the high-performance pump-out system for maintaining the low residual pressure level in the vacuum chamber during operation of the source. It is crucial to maintain the low residual pressure level in the chamber when the LPS operates with the gas-jet Xe target, since the Xe atoms have a wide absorption band within the EUV range [5].

The main elements of the vacuum pump-out system are the three turbomolecular pumps (TMP) KYKY CXF-320/3001 of performance of 3000 l/s. Thus, total performance of the pump-out system is about 9000 l/s.

Fig. 5 shows the measured dependences of the residual pressure level in the vacuum chamber on the Xe pressure at a conical nozzle inlet with $d_{cr} = 500\,\mu$m at various durations of a pulse of opening of the nozzle pulse valve (the variable B in Fig. 5). In these experiments, a valve opening rate coincided with the laser-pulse repetition rate and was 10 Hz. It is clear that within the pressure range 2–12 bar, when the duration of the pulse of opening of the nozzle is about 400 μs, the residual pressure level in the chamber is 10^{-3} Torr. According to the tabular data from [16], absorption of EUV radiation with the wavelength of 11.2 nm by residual Xe is 8 % in these conditions in our test stand (the distance from the spark to the EUV radiation detector is about 1 m).

Due to high Xe cost and its high flowrates during operation of the source, it is planned to retrofit the stand with a Xe recirculation system in the future. Using the recirculation system, the gas that is pumped out by the

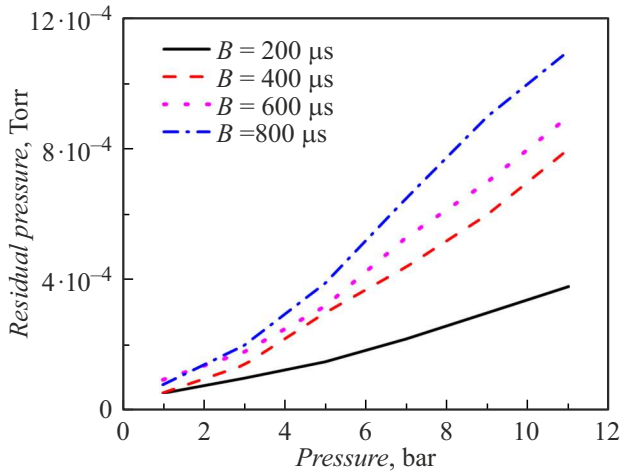

Figure 5. Results of measurement of the residual pressure level in the vacuum chamber in a dependence on the gas pressure at the nozzle inlet.

vacuum pumps out of the chamber volume will be pumped into a special bottle instead of being discharged into an exhaust trunk line. It will allow reusing the accumulated gas in the future when the source operates.

1.4. EUV radiation diagnostics system

Now, the EUV radiation diagnostics system includes the following main instruments: the mirror spectrometer, the double-mirror monochromator and the EUV imaging system.

The mirror spectrometer is designed for recording emission spectra of the laser plasma within the range 3–30 nm and for measuring intensity of radiation in absolute units. The operation of the instrument is based on Bragg reflection of EUV radiation from the multilayer X-ray mirrors. A polychromatic beam of radiation of the laser plasma is incident to the MXM at a certain grazing angle φ and after that the MXM reflects radiation in a quite narrow spectral band $\lambda_0 \pm \Delta\lambda$. The spectrum is scanned by rotating the MXM on a goniometer platform in relation to incident radiation, while the detector is synchronously rotated by a double angle. Semiconductor diodes FDUK-100UV calibrated at the synchrotron were used as a detector [17]. Operation of an X-ray signal detection system is synchronized with operation of a laser system shutter by means of a control and synchronization unit. Thus, the intensity of EUV radiation of the laser plasma is measured, wherein the intensity corresponds to one pulse of a pumping laser. The signal values recorded by the detector are retained in a text file as a numerical table. During the experiments described in the present study, the spectrometer had an MXM based on the Mo/Be- structure installed and an operating range of the wavelengths of this mirror was 11–18 nm. At the wavelength $\lambda_0 = 11.2$ nm reflectance is $R = 0.52$, while spectrum selectivity is $\Delta\lambda/\lambda_0 = 0.04$. A level of the noise signal was reduced by using two Zr/Ru free-hanging film filters. Reflectances of the multilayer mirrors and transmission coefficients of the filters in the EUV ranges were calibrated in a high-resolution reflectometer [18].

More details about the design, the characteristics and the operating principles of the spectrometer can be found in the paper [19]. All the elements of the instrument are calibrated, thereby making it possible to measure the intensity of radiation in absolute units. We evaluate an error of the absolute measurements at the level of 15 %.

The double-mirror monochromator is designed to measure intensity of radiation in absolute units within a narrow spectral band of 2 %. Operation of the instrument is also based on Bragg radiation from the MXM, wherein it is reflected from two serial mirrors, thereby making it possible to select a narrower spectral band. An incident angle of radiation to the surface of each of the mirrors is 7°. At the same time, it is impossible to scan the spectrum. A set of the Mo/Si- mirrors was synthesized for this instrument, and the reflectance for the double-mirror diagram at the wavelength of $\lambda_0 = 11.2$ nm is $R = 0.045$, while the spectrum selectivity is $\lambda/\lambda_0 = 0.02$. The FDUK-100EF photodiode is used as a detector. In the same way as for the mirror spectrometer, operation of the detection system is synchronized with operation of the laser system shutter. The measured intensity of plasma radiation at the wavelength of 11.2 nm corresponds to one pulse of the pumping laser. The selected spectral band corresponds to the spectral band of an optical system of the designed new-generation EUV lithograph. The instrument is described in detail in the paper [20].

The EUV imaging system is designed for recording images of a radiating area of the laser spark within the EUV range and measuring sizes of the radiating area with high spatial resolution. A main assembly of the imaging system is a Schwarzschild lens. The lens consists of a convex and a concave spherical mirror. The main advantage of the Schwarzschild diagram is that it uses multi-layer X-ray normal-incidence optics. This solution can eliminate spherical aberration and astigmatism, which are typical for X-ray optical diagrams with using single MXMs [21–23] as well as obtain high light intensity, spectral and spatial resolution. A set of the highly-reflective normal-incidence MXMs based on Mo/Be was synthesized for this lens. Besides, the Mo/Be- film filters were also manufactured for the imaging system. The radiation detector is a CMOS-matrix with a pixel array 2048×2048, wherein the size of one pixel is $6.5 \times 6.5\,\mu$m. The system allows obtaining the images of the laser spark at the wavelength of 11.25 nm with five times magnification. The instrument FOV is a square with the side of 13.3 mm. The high spatial resolution of about $4\,\mu$m allows not only determining the sizes of the radiating area with high accuracy, but also recording heterogeneity of spatial resolution of intensity of EUV radiation of the plasma cloud. The high reflectances of the MXMs, transmission coefficients

of the film filters as well as sensitivity of the matrix detector allow obtaining the images of the laser spark, which correspond to one pulse of the pumping laser. A design of the instrument, procedures of manufacturing the optical elements as well as the first results obtained by means of the imaging system are described in detail in the paper [24].

Besides, as noted above, the experimental stand is planned to be used to investigate the ion fluxes that originate during LPS operation, to investigate degradation of the multi-layer X-ray optics under effect of the ions and nozzle destruction products.

2. First experimental results

The optical system was pre-adjusted by recording emission spectra of carbon dioxide. In accordance with the paper [25,26], within the studied range of the wavelengths 11–18 nm, narrow and quite bright emission lines of the ions of oxygen O VI are observed when the plasma cloud is formed in the carbon dioxide target. Fig. 6 shows the carbon dioxide target spectrum that is recorded in the stand described herein after necessary adjustments of the optical system.

As expected, the spectrum exhibited four prominent peaks that correspond to radiation of the ions of oxygen O VI at the wavelengths 11.64, 12.98, 15, 17.3 nm. A position of maximums of the peaks in the spectrum well complies with the tabular values of the wavelengths [27].

The main studies that have been carried out in the test stand are dedicated to measuring intensity of radiation of the xenon laser system at the wavelength of 11.2 nm. Fig. 7 shows a spectrum of radiation of the Xe laser plasma, which is recorded by means of the mirror spectrometer. The recorded spectrum exhibits a bright maximum of intensity of radiation at the wavelength of 11.2 nm. According to the papers [12, 28–30], the recorded radiation corresponds to

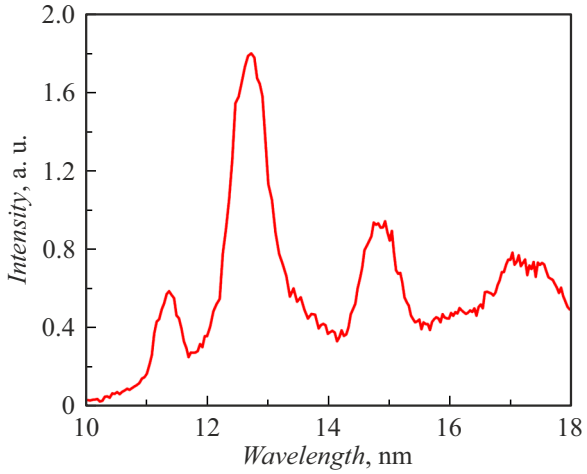

Figure 6. Spectrum of radiation of the carbon dioxide laser plasma, which is obtained by means of the mirror spectrometer.

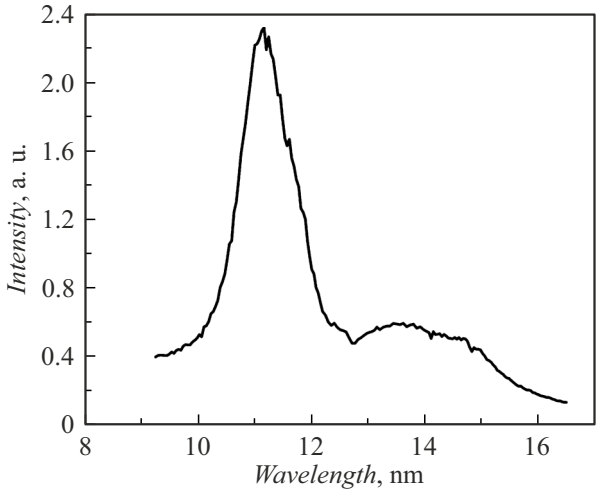

Figure 7. Spectrum of radiation of the Xe laser plasma, which is recorded in the mirror spectrometer.

the UTA band. In our case, there is a shift of the position of the observed maximum of radiation due to an absorption edge of Be included in the used MXM, at the wavelength of 11.1 nm. In this experiment, the gas pressure at the nozzle inlet was 8 bar. The plasma was excited by the acutely focused laser ray and the pulse energy was 0.7 J. The distance from the focus point to the nozzle edge is 0.6 mm.

The optimal parameters of LPS operation were determined by investigating dependences of conversion efficiency of LPS at the wavelength of 11.2 nm on the distance between the focus point and the nozzle edge, the gas pressure at the nozzle inlet, the laser pulse energy and the size of the laser beam in an area when radiation interacts with the target.

Fig. 8 shows the obtained dependence of conversion efficiency of the source when radiating into a solid angle of 2π sr within the spectral band (11.2 ± 0.22) nm (hereinafter we name this band a 4 % spectral band, and the respective conversion efficiency $CE_{2\pi,4\%}$) on the distance between the focus point of laser radiation and the nozzle edge. In these experiments, the nozzle was moved in the slide along a one's own axis, wherein two other coordinates remain fixed. The gas pressure was 8 bar, the laser pulse energy was 0.7 J with point beam focusing of the laser ray (the beam diameter within the interaction area is about $d = 25\,\mu$m). Due to proximity of the absorption edge of Be to the working wavelength of 11.2 nm as well as a decline of intensity of the emission line when moving away from the resonance wavelength (as can be seen in Fig. 6), the spectral band recorded by the mirror is below 4 %, therefore, the values of $CE_{2\pi,4\%}$ given herein shall be considered as its lower estimate.

It is clear from the presented dependence that when the focus point of laser radiation is moved away from the nozzle edge, CE is significantly reduced. It is due to reduction

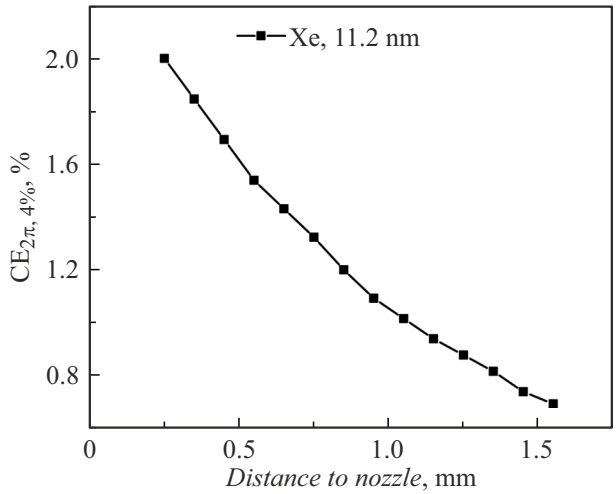

Figure 8. Dependence of conversion efficiency on the distance between the focusing point of laser radiation and the nozzle butt-end.

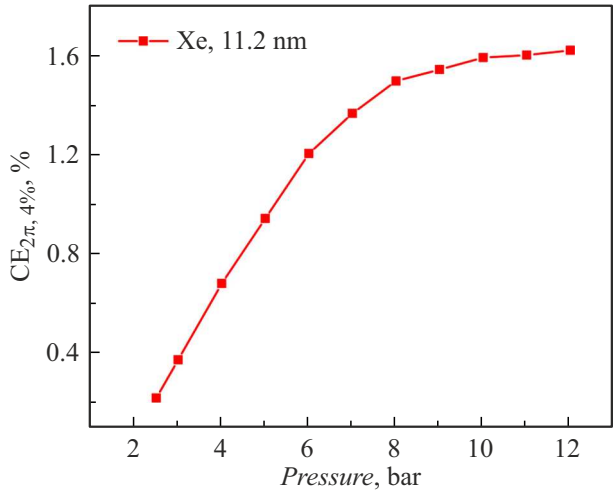

Figure 9. Dependence of conversion efficiency on the gas pressure at the nozzle inlet.

of a density of Xe particles in the area where the target interacts with laser radiation. Results of these experiments were taken to select a basic value of the distance between the focus point and the nozzle edge as $z_0 = 0.6$ mm. Thus, the area of formation of the laser plasma was removed quite far from the nozzle so as to reduce its degradation under effect of the ions flying away out of the plasma cloud. At this, the value of conversion efficiency is still quite high.

Fig. 9 shows the obtained dependence of CE on the gas pressure at the nozzle inlet for the 4% spectral band (the measurements were carried out in the mirror spectrometer).

In these experiments, the laser pulse energy was also 0.7 J with point beam focusing of the laser ray (the beam diameter within the interaction area is about 25 μm). The distance to the nozzle exit is 0.6 mm. It is clear in the dependence that with increase of the gas pressure at the nozzle inlet CE significantly increases. At the pressure above 10 bar the dependence reaches saturation. At the pressure of 12 bar the obtained conversion efficiency $CE_{2\pi,4\%} = 1.6\%$.

Fig. 10 shows the measured dependence of CE on the laser pulse energy. Below, the total energy of one laser pulse is plotted along the abscissa axis. The top has a value of the energy reaching the area of interaction with the target, which corresponds to each of the measurements.

The experiments were carried out when the gas pressure at the nozzle inlet was 12 bar and the laser beam had point beam focusing. The distance to the nozzle exit was 0.6 mm. As it is clear from the shown dependence, with increase of the laser pulse energy the value of $CE_{2\pi,4\%}$ increases. With increase of the pulse energy above 0.4 J (in this case, about 0.3 J/pulse reaches the area of interaction with the target), the increase of the value of $CE_{2\pi,4\%}$ is somewhat decelerated.

Fig. 11 shows the measured $CE_{2\pi,4\%}$ with the various sizes of the laser beam in the area of interaction with the target. In this experiment, the focusing lens was moved along the focus axis of the system, thereby moving the system focus point and changing the size of the laser beam in the area of interaction with the target (in the area of the maximum density of the gas jet).

In the shown dependence, a lens coordinate that is equal to zero corresponds a position, in which the focus point of the optical system is exactly under the nozzle exit (the respective diameter of the laser beam is 25 μm). Thus, it is clear that the maximum of $CE_{2\pi,4\%}$ is observed with a certain shift in relation to the „zero position“. The maximum of conversion efficiency is observed when the converging laser beam of the diameter of 60 μm interacts with the target. With further increase of the diameter of the laser beam, there is decrease of the value of $CE_{2\pi,4\%}$. The

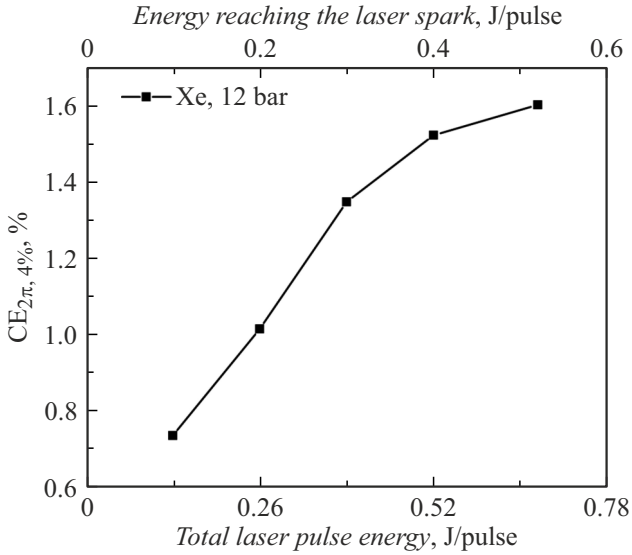

Figure 10. Dependence of conversion efficiency on the laser pules energy.

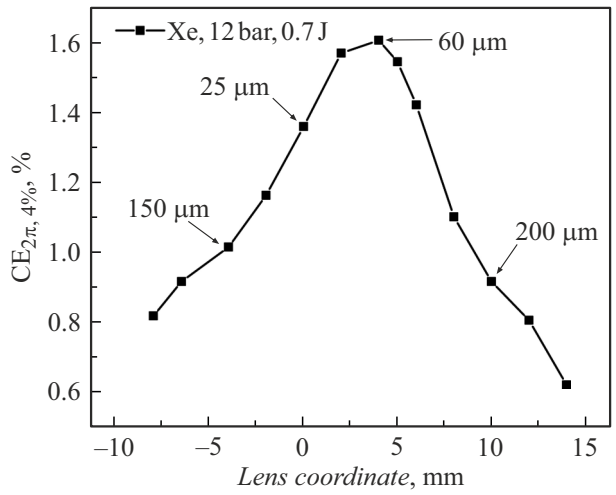

Figure 11. Conversion efficiency at various positions of the focusing lens.

decrease of conversion efficiency is also observed in the case of interaction of the diverging laser beam with the target.

Separately, conversion efficiency of the source was measured using the double-mirror monochromator within the 2 % spectral band. The measurements were carried out at the optimal value of the gas pressure, which was 12 bar, the laser pulse energy of 0.7 J and at the various distances from the focus point of laser radiation to the nozzle edge. The distances from the nozzle edge were selected to be $z = 0.6$, 0.4 and 0.2 mm. Thus, it can be said that by significantly reducing the residual pressure level in the vacuum chamber of the installation and using the long-focus optical system, conversion efficiency of LPS is significantly increased (by 30 %–40 %).

Conclusion

The study included designing, manufacturing and commissioning the test stand designed to investigate the characteristics of the powerful EUV radiation LPSes. The main advantage of this stand is that it is equipped with the high-performance pump-out system. The presence of this pump-out system allows obtaining the sufficient residual pressure level in the vacuum chamber (at most 10^{-3} Torr) with the high flowrates of the working gas. As shown in the paper [31], when using the pump-out systems of the TMPs with total performance of about 9000 l/s, it is possible to achieve the residual pressure level in the chamber of at most 10^{-3} Torr by using the conical nozzles of the critical diameter of about 250 μm without the pulse valve. Thus, the stand allows carrying out the studies in conditions that are as close as possible to the conditions of operation of the designed new-generation lithographic machines (the high laser pulse repetition frequency, above 1 kHz; continuous outflow of the gas through the nozzle without using the pulse valve).

The first results of operation of the described stand were the studied dependences of CE of the LPS with the gas-jet Xe target at the wavelength of 11.2 nm on the distance between the focusing point of the laser beam of and the nozzle edge, the gas pressure, the laser pulse energy and the focusing spot size. The recorded conversion efficiency of the source into a half space to the 4 % spectral band achieves $CE_{2\pi,4\%} = 2\%$ as its lower estimate.

Funding

The test stand was manufactured under the state assignment FFUF-2024-0022. The experimental studies were supported by the grant from the Russian Science Foundation № 21-72-30029-P.

Conflict of interest

The authors declare that they have no conflict of interest.

References

[1] S. Bajt. J. Vacuum Sci. Technol. A: Vacuum, Surfaces, and Films, **18** (2), 557 (2000).
[2] R.M. Smertin, N.I. Chkhalo, M.N. Drozdov, S.A. Garakhin, S.Yu. Zuev, V.N. Polkovnikov, N.N. Salashchenko, P.A. Yunin. Opt. Express, **30** (26), 46749 (2022).
[3] R. Smertin, N. Chkhalo, S. Garakhin, V. Polkovnikov, S. Zuev. Opt. Lett., **49** (13), 3690 (2024).
[4] N.I. Chkhalo. Mikroelektronika, **53** (5), 375 (2024) (in Russian).
[5] R. de Bruijn, K. Koshelev, G. Kooijman, E.S. Toma, F. Bijkerk. J. Quant. Spectr. Radiative Transfer, **81** (1-4), 97 (2003).
[6] R. de Bruijn, K. Koshelev, F. Bijkerk. J. Phys. D: Appl. Phys., **36** (18), L88 (2003).
[7] A.N. Nechay, A.A. Perekalov, N.N. Salashchenko, N.I. Chkhalo. Opt. i spektr., **129** (3), 266 (2021) (in Russian).
[8] S.G. Kalmykov, P.S. Butorin, M.E. Sasin. J. Appl. Phys., **126** (10), 103301 (2019).
[9] V.E. Guseva, A.N. Nechay, A.A. Perekalov, N.N. Salashchenko, N.I. Chkhalo. Appl. Phys. B, **129** (10), 155 (2023).
[10] G.D. Kubiak, L.J. Bernardez II, K.D. Krenz. Emerging Lithographic Technol. II. – SPIE, **3331**, 81 (1998).
[11] P.S. Butorinov, Y.M. Zadiranov, S.Yu. Zuev, S.G. Kalmykov, V.N. Polkovnikov, M.E. Sasin, N.I. Chkhalo. ZhTF, **88** (10), 1554 (2018) (in Russian).
[12] E.B. Saloman. J. Phys. Chem. Reference Data, **33** (3), 765 (2004).
[13] K. Mann, J. Holburg, S. Lange, M. Müller, B. Schäfer. EUV Lithography X – SPIE, **10957**, 305 (2019).
[14] V.E. Guseva, D.S. Dmitriev, A.N. Nechai, A.A. Perekalov, A.K. Chernyshev, N.I. Chkhalo. Mater. XXIX Mezhdunar. simp. „Nanofizika i nanoelektronika“. (2025) (in Russian).

[15] S.S. Morozov, S.A. Garakhin, M.V. Zorina, B.A. Ulasevich, N.I. Chkhalo, D.G. Reunov, M.Yu. Znamenskii. Mater. XXIX Mezhdunar. Simp. „Nanofizika i nanoelektronika“. (2025) (in Russian).
[16] Electronic source. Available at: https://henke.lbl.gov/optical_constants/
[17] P.N. Aruev, M.M. Barysheva, B.Ya. Ber, N.V. Zabrodskaya, V.V. Zabrodskii, A.Ya. Lopatin, A.E. Pestov, M.V. Petrenko, V.N. Polkovnikov, N.N. Salashchenko, V.L. Sukhanov, N.I. Chkhalo. Kvant. elektron., **42** (10), 943 (2012) (in Russian).
[18] S.A. Garakhin, N.I. Chkhalo, I.A. Kas'kov, A.Ya. Lopatin, I.V. Malyshev, A.N. Nechay, A.E. Pestov, V.N. Polkovnikov, N.N. Salashchenko, M.V. Svechnikov, N.N. Tsybin, I.G. Zabrodin, S.Yu. Zuev. Rev. Sci. Instrum., **91** (6), 063103 (2020).
[19] A.V. Vodop'yanov, S.A. Garakhin, I.G. Zabrodin, S.Yu. Zuev, A.Ya. Lopatin, A.N. Nechai, A.E. Pestov, A.A. Perekalov, R.S. Pleshkov, V.N. Polkovnikov, N.N. Salashchenko, B.A. Ulasevitch, N.I. Chakhalo. Kvant. elektron., **51** (8), 700 (2021) (in Russian).
[20] N.I. Chkhalo, S.V. Golubev, D. Mansfeld, N.N. Salashchenko, L.A. Sjmaenok, A.V. Vodopyanov. J. Micro/Nanolith. MEMS MOEMS, **11**, 021123 (2012).
[21] J. Holburg, M. Muller, K. Mann, S. Wieneke. J. Vacuum Sci. Technol. A: Vacuum, Surfaces, and Films, **37** (3), 031303 (2019). DOI: 10.1116/1.5082906
[22] V.E. Levashov, K.N. Mednikov, A.S. Pirozhkov, E.N. Ragozin. Kvant. elektron., **36** (6), 549 (2006) (in Russian).
[23] V.G. Kapralov, R. Korde, V.E. Levashov, A.S. Pirozhkov, E.N. Ragozin. Kvant. elektron., **32** (2), 149 (2002) (in Russian).
[24] A.A. Perekalov, V.E. Guseva, I.V. Malyshev, A.N. Nechay, A.E. Pestov, D.G. Reunov, R.M. Smertin, M.N. Toropov, N.N. Tsybin, N.I. Chkhalo. Opt. Laser Technol. accepted for publication.
[25] H. Fiedorowicz, A. Bartnik, M. Szczurek, H. Daido, N. Sakaya, V. Kmetik, T. Wilhein. Opt. Commun., **163** (1-3), 103 (1999).
[26] A.N. Nechay, A.A. Perekalov, N.I. Chkhalo, N.N. Salashchenko. ZhTF, **89** (11), 1656 (2019) (in Russian).
[27] R.L. Kelly, L.P. Palumbo. *Atomic and ionic emission lines below 2000 angstroms: hydrogen through krypton* (Naval Research Laboratory, Washington D.C., 1973)
[28] S. Kranzusch, K. Mann. Opt. Commun., **200** (1-6), 223 (2001).
[29] H. Fiedorowicz, A. Bartnik, R. Jarocki, J. Kostecki, J. Krzywiński, J. Mikołajczyk, M. Szczurek. J. Alloys Compounds, **401** (1-2), 99 (2005).
[30] H. Tanuma, H. Ohashi, S. Fujioka, H. Nishimura, A. Sasaki, K. Nishihara. J. Phys.: Conf. Series. – IOP Publishing, **58** (1), 231 (2007).
[31] N.G. Korobeishchikov, I.V. Nikolaev, M.A. Roenko. Nuclear Instruments and Methods in Physics Research Section B: Beam Interactions with Materials and Atoms, **438**, 1 (2019).

Translated by M.Shevelev